JOURNAL OF GEOPHYSICAL RESEARCH, VOL. 107, NO. D10, 10.1029/2001JD000642, 2002

Diurnal variation in water vapor over North America and its implications for sampling errors in radiosonde humidity

Aiguo Dai and Junhong Wang
National Center for Atmospheric Research, Boulder, Colorado, USA

Randolph H. Ware and Teresa Van Hove
GPS Science and Technology Program, University Corporation for Atmospheric Research, Boulder, Colorado, USA

Received 21 March 2001; revised 10 September 2001; accepted 10 September 2001; published 22 May 2002.

[1] Diurnal variations in atmospheric water vapor are studied by analyzing 30-min-averaged data of atmospheric precipitable water (PW) for 1996–2000 derived from Global Position System (GPS) observations from 54 North America stations. Vertical structures in the diurnal cycle of atmospheric water vapor are examined using 3-hourly radiosonde data from Lamont, Oklahoma, during the 1994–2000 period. Significant diurnal variations of PW are found over most of the stations. The diurnal (24 hour) cycle, S_1, which explains over 50% of the subdaily variance, has an amplitude of 1.0–1.8 mm over most of the central and eastern United States during summer and is weaker in other seasons. The S_1 peaks around noon in winter and from midafternoon to midnight in summer. The semidiurnal (12 hour) cycle is generally weak, with an amplitude of a few tenths of 1 mm. At Lamont, specific humidity in the free troposphere is significantly higher in the early morning (0000–0008 local solar time (LST)) than during the day (0800–1800 LST). This diurnal variation changes little from ~4 to 16 km above the ground. Near the surface, specific humidity tends to be lower in the morning than in the afternoon and evening in all seasons except summer. This near-surface diurnal cycle propagates upward through the lower troposphere (up to ~4 km). Errors in seasonal mean humidity due to undersampling the diurnal cycle with twice-daily synoptic soundings (at 0000 and 1200 UTC) are generally small (within ±3% or ±0.5 mm for PW), but it can easily reach 5–10% if there is only one random sounding per day. Several physical processes are proposed that could contribute to the diurnal variations in atmospheric water vapor. *INDEX TERMS:* 3300 Meteorology and Atmospheric Dynamics; 1655 Global Change: Water cycles (1836); 6969 Radio Science: Remote sensing; *KEYWORDS:* water vapor, diurnal cycle, GPS

1. Introduction

[2] Water vapor plays a key role in atmospheric radiation and hydrological cycle. Observations of atmospheric water vapor are traditionally made through balloon-borne radiosondes. However, radiosonde observations are usually available only twice a day and only at limited locations (at 700–800 land stations, mostly in the Northern Hemisphere) [*Wang et al.*, 2000]. Since atmospheric water vapor is highly variable in both time and space (e.g., associated with summer thunderstorms), the radiosonde observations are obviously insufficient for studying the variations of atmospheric water vapor at various temporal and spatial scales. Recently, satellite measurements of water vapor began to improve the spatial coverage, especially over the oceans [*Randel et al.*, 1996], but the temporal sampling still remains poor. Because of this, there have been few global or regional analyses of diurnal variations of atmospheric water vapor, even though the diurnal variations could affect surface and atmospheric longwave radiation and atmospheric absorption of solar radiation (and thus have implications for atmospheric pressure tides [*Dai and Wang*, 1999]). (Here, diurnal or subdaily variations refer to all variations with a time period of $\leq$24 hours, while the diurnal cycle refers to a diurnal (sine) harmonic with a period of 24 hours.) Diurnal variations of water vapor are also related to many other processes such as diurnal variations in moist convection and precipitation [*Dai et al.*, 1999a; *Dai*, 2001], surface wind convergence [*Dai and Deser*, 1999], and surface evapotranspiration.

[3] The Global Positioning System (GPS) consists of a network of 24 satellites that transmit radio signals to a large number of users engaged in navigation, time transfer, and relative positioning [*Leick*, 1990]. These L-band radio signals are delayed, in part, by atmospheric water vapor (referred to as wet delay) as they travel from GPS satellites to ground-based GPS receivers. Since the early 1990s, methods have been developed to use the wet delay data from GPS receivers to retrieve atmospheric column-integrated water vapor or precipitable water (PW) [e.g., *Bevis et al.*, 1992, 1994; *Rocken et al.*, 1993, 1997], "slant water" [*Ware et al.*, 1997], and 3-dimensional (3-D) water vapor [*MacDonald et al.*, 2002]. GPS-sensed PW is found to have an accuracy (RMS error) ranging from better than 2 mm in North America [*Rocken et al.*, 1993, 1997; *Duan et al.*, 1996; *Fang et al.*, 1998] and Australia [*Tregoning et al.*, 1998] to 2.2 mm in Taiwan [*Liou et al.*, 2001] and 3.7 mm in Japan [*Ohtani and Naito*, 2000]. These RMS errors are comparable to those of radiosonde and microwave radiometer measurements [*Tregoning et al.*, 1998; *Lijegren et al.*, 1999]. Unlike microwave radiometers, however, GPS receivers work under all weather conditions. Other advantages of GPS-sensed PW include high sampling resolution (every few minutes or better), self-calibration, low cost, and large coverage [*Ware et al.*, 2000].

[4] Here we study the mean diurnal variations in atmospheric precipitable water by analyzing 30-min-averaged data of GPS-sensed PW for the 1996–2000 period from 54 GPS sites in North America. Vertical structures of the diurnal cycle of atmospheric

0148-0227/02/2001JD000642$09.00

water vapor are examined by analyzing 3-hourly sounding data from Lamont, Oklahoma. Diurnal sampling errors in synoptic humidity soundings are also estimated using the GPS PW data. The PW data are compared with diurnal cycles in precipitation to investigate the causes of PW diurnal variations.

2. Data and Analysis Method

2.1. GPS-Sensed PW Data

[5] Since 1996, near-real-time GPS tracking data, together with surface meteorological data, have been obtained from a number of GPS stations (Table 1) operated by the National Oceanic and Atmospheric Administration Forecast Systems Laboratory and National Geodetic Service. The GPS data for the 1996–2000 period from 54 U.S. stations were used in this study. Most of the stations do not have data for 1996, and many have gaps (mainly due to missing meteorological data) during the study period.

[6] The GPS receivers record tracking data from 7–8 satellites in view every 30 s. Starting from these instantaneous measurements, we first checked and removed any abnormal (e.g., out of range) data points. We then sampled these quality-controlled GPS data at 120-s intervals. Path delays were then derived from the sampled GPS tracking data using the Bernese v4.2 software (*Beutler et al.* [1996] and updates) with satellite orbit solutions from the Center for Orbit Determination in Europe for 1996–1999 and from International GPS Service rapid orbits for 2000 on. These path delay data (with a 120-s sampling interval) were used to derive the 30-min-averaged path delay using a cutoff elevation angle of 7°. The wet path delay induced by water vapor was obtained by subtracting the hydrostatic delay (using the Saastamoinen model [*Saastamoinen*, 1972] for data before 2000 and using the dry mapping function of *Niell* [1996] for 2000) from the total path delay (note that the GPS data were processed at different times, and the processing procedure has evolved over the years). The wet path delay was mapped into zenith wet delay (ZWD) using the wet mapping function of *Niell* [1996]. The ZWD was converted into atmospheric precipitable water using the π parameter [*Bevis et al.*, 1992, 1994]. Station air temperature (T_s) was used to estimate the weighted atmospheric mean temperature (T_m, used to compute π) using a local $T_m - T_s$ relationship for stations LMNO, VCIO, PRCO, HKLO, and PLTC (where local sounding and T_s data were available for deriving the local relationship). The $T_m - T_s$ relationship of *Bevis et al.* [1994] was used for all the other stations. More technical details for computing PW are given in Appendix A.

[7] Ocean tidal loading effects were not included in calculating the PW before year 2000 (it was included in 2000 PW calculations). (Ocean tides redistribute oceanic masses and cause vertical crustal displacements in the millimeter to centimeter range at ground-based GPS sites. The effect of this displacement on GPS-sensed PW is often referred to as the ocean tidal loading effect.) We found that the ocean loading effect can cause large (up to ±2.0–3.0 mm) errors in 30-min-averaged PW and can cause substantial differences in mean diurnal variations over the Pacific and Atlantic coastal United States. To minimize these errors, we computed the ocean-loading-induced vertical site displacements and used linear regression equations (of the displacement and the associated PW error derived from the 2000 data) to account for the ocean loading effect for the PW data before 2000 at all the stations. Tests using 2000 PW data showed that the correction using the regression relationship yielded PW similar to that computed with ocean loading included in the original calculation.

2.2. Other Data

[8] In order to evaluate the GPS PW data, we derived PW from a ground-based microwave radiometer (MWR) [*Solheim et al.*, 1998] and from radiosondes at the Atmospheric Radiation Measurement Program Cloud and Radiation Testbed (ARM/CART) site (central facility) near Lamont, Oklahoma, where GPS-sensed PW data were also available. The MWR and radiosonde data were obtained during several intensive operational periods (i.e., 1–25 April 1997, 23 June through 16 July 1997, 16 September through 10 October 1997, and January 1998). During these periods the MWR measurements were made at hourly intervals [*Han and Westwater*, 1995], while the soundings were available 8 times per day. We interpolated the 30-min GPS data onto the MWR and radiosonde sampling times and then compared the instantaneous measurements and the mean diurnal variations in these PW data. Three-hourly vertical profiles of atmospheric humidity obtained from radiosondes during the 1994–2000 period at the ARM/CART site were also used to derive seasonal mean diurnal variations of atmospheric specific humidity from the surface to 16 km in altitude. The radiosonde humidity data for 1996–1998 (used for comparison with the GPS data) were corrected for the dry bias in Vaisala sondes [*Lesht*, 1999; *Guichard et al.*, 2000; *Wang et al.*, 2002].(The relative humidity profile was scaled using an algorithm developed by Vaisala and the National Center for Atmospheric Research to account for a dry bias. The correction algorithm is a function of age of the sonde and the relative humidity.) The dry bias has not yet been corrected for the other years (used in Figure 7 only) and should only have minor effects because the data were normalized by standard deviation.

[9] For comparison with the PW diurnal variations, we derived mean diurnal variations of precipitation at the GPS sites in the contiguous United States from a gridded hourly precipitation data set for the 1963–1993 period [*Higgins et al.*, 1996]. The hourly precipitation data showed the spatial patterns in the diurnal cycle of precipitation over the United States [*Dai et al.*, 1999a]. The NASA Water Vapor Project Data Set (NVAP) [*Randel et al.*, 1996] for 1988–1995 was also used for comparison with the seasonal mean PW derived from the GPS data. The NVAP data are a combination of radiosonde and satellite (TOVS and SSM/I) observations.

2.3. Diurnal Analysis Method

[10] The 30-min-averaged data of GPS-sensed PW were first converted into diurnal anomalies by removing the daily mean for each day (days with more than one third of the observations missing were excluded from the analysis). The diurnal anomalies were then averaged over each season and all years to obtain seasonal mean diurnal anomalies. We tried various other methods for deriving the mean diurnal anomalies, including high-pass filtering the 30-min data. We found that the above method worked best for these GPS data with relatively short record length and many missing gaps. Applying high-pass filtering to the diurnal anomalies before averaging did not make noticeable changes to the results. Since many of the stations only have data for 1999–2000 (Table 1), the mean diurnal variations derived here may differ slightly from those of long-term (e.g., 10–20 year) averages.

[11] The mean diurnal anomalies (with a sampling interval of 30 min) of PW for each season at each GPS station were then subjected to a harmonic analysis. The mean diurnal variations may be represented by

$$\mathrm{PW}(t') = \mathrm{PW}_0 + \sum_{n=1}^{4} S_n(t') + R \qquad (1)$$

$$S_n(t') = A_n \sin(nt' + \sigma_n) = a_n \cos(nt') + b_n \sin(nt'), \qquad (2)$$

where S_n, n = 1, 2, 3, and 4, denotes harmonics with periods of 24, 12, 8, and 6 hours, respectively; PW_0 is the daily mean value; R is the residual; A_n is the amplitude (note that the peak-to-peak amplitude is $2A_n$); σ_n is the phase; and t' is mean local solar time (LST) expressed in degrees or radians (i.e., $t' = 2\pi t_1/24$, where t_1 is LST in hours). The residual in (1) contains the higher-order harmonics of the diurnal variations. In the following, we will show

Table 1. Station Information[a]

Stn	Lon, Lat	A1, P1	A2, P2	Var	Err	DP	Location
ARP3	−97.1, 27.8	0.73, 8.00	0.11, 10.50	93	−0.29	1998–2000	Aransas Pass, Tex.
AZCN	−107.9, 36.8	0.46, 0.50	0.26, 9.75	93	−0.54	1999–2000	Aztec, N. M.
BLKV	−80.4, 37.2	0.83, 17.25	0.70, 1.00	88	−2.57	1999–2000	Blacksburg, Va.
BLMM	−90.0, 36.9	0.90, 18.00	0.43, 0.75	92	−0.60	1999–2000	Bloomfield, Mo.
BLRW	−90.5, 43.2	1.06, 19.00	0.30, 0.50	97	−1.50	1999–2000	Blue River, Wis.
CCV3	−80.5, 28.5	0.86, 17.00	0.37, 10.75	92	−0.36	1998–2000	Cape Canaveral, Fla.
CENA	−144.7, 65.5	0.27, 20.50	0.55, 10.00	81	−2.56	1998–2000	Central, Alaska
CHA1	−79.8, 32.8	0.83, 20.50	0.25, 1.50	91	−0.63	1998–2000	Charleston, S. C.
CLK1	−98.0, 44.9	0.98, 20.75	0.21, 2.25	77	−0.39	1999–2000	Clark, S. D.a
CNWM	−92.7, 37.5	0.89, 17.00	0.09, 0.75	97	0.03	1999–2000	Conway, Mo.
DQUA	−94.3, 34.1	0.87, 15.75	0.17, 2.50	98	−0.07	1997–2000	Dequeen, Ark.
DRV1	−76.6, 37.0	0.79, 15.75	0.35, 2.25	68	−0.88	1999–2000	Driver, Va.
EKY1	−82.8, 27.6	0.14, 20.25	0.02, 6.50	53	0.15	1998–1999	Egmont Key, Fla.
ENG1	−89.9, 29.9	1.26, 16.00	0.21, 5.00	98	0.30	1998–2000	English Turn, La.
FBYN	−97.3, 40.1	0.56, 16.25	0.39, 1.50	82	−0.46	1999–2000	Fairbury, Nebr.
FMC1	−76.7, 34.7	0.91, 19.00	0.20, 11.75	98	−0.57	1999–2000	Fort Macon, N. C.
GAL1	−94.7, 29.3	0.81, 10.25	0.14, 5.50	94	0.29	1998–2000	Galveston, Tex.
GDAC	−102.2, 37.8	1.26, 20.50	0.19, 0.25	99	−0.53	1997–2000	Granada, Colo.
GNAA	−146.0, 62.1	0.12, 10.75	0.67, 10.00	81	−2.08	1998–2000	Glennallen, Alaska
HBRK	−97.3, 38.3	0.36, 17.50	0.17, 3.25	97	0.27	1996–2000	Hillboro, Kans.
HKLO	−95.9, 35.7	0.68, 12.25	0.18, 2.25	97	0.01	1996–2000	Haskell, Okla.
HVLK	−99.1, 37.7	0.63, 19.50	0.31, 2.25	98	−0.01	1997–2000	Haviland, Okla.
JTNT	−101.0, 33.0	0.39, 16.25	0.02, 4.50	97	0.07	1997–2000	Jayton, Tex.
KYW1	−81.7, 24.6	0.50, 15.25	0.20, 10.00	94	−0.03	1998–2000	Key West, Fla.
LMNO	−97.5, 36.7	0.39, 17.25	0.13, 2.75	86	0.21	1996–2000	Lamont, Okla.
LTHM	−94.2, 39.6	0.89, 14.25	0.15, 3.25	93	0.32	1999–2000	Lathrop, Mo.
MBWW	−106.2, 41.9	0.87, 20.75	0.17, 10.25	97	−0.56	1999–2000	Medicine Bow, Wyo.
MIA3	−80.2, 25.7	1.79, 17.25	0.52, 9.00	93	0.45	1999–2000	Miami, Fla.
MOB1	−88.0, 30.2	0.54, 19.25	0.40, 8.75	90	0.33	1998–2000	Mobile, Ala.
MOR1	−72.7, 40.8	1.25, 20.75	0.35, 2.00	92	−1.02	1999–2000	Moriches, N. Y.
MRRN	−101.7, 42.9	0.85, 19.00	0.10, 11.50	98	−0.17	1999–2000	Merriman, Nebr.
NDBC	−89.6, 30.4	1.07, 16.50	0.17, 0.25	99	−0.41	1996–2000	Stennis Space Center, Miss.
NDSK	−95.6, 37.4	0.50, 15.50	0.15, 3.00	96	0.11	1997–2000	Neodesha, Nebr.
NLGN	−97.8, 42.2	0.91, 17.25	0.14, 2.25	95	0.22	1999–2000	Neligh, Nebr.
OKOM	−88.9, 34.1	1.35, 15.25	0.35, 1.25	95	−1.29	1999–2000	Okolona, Miss.
PATT	−95.7, 31.8	0.78, 17.25	0.33, 1.75	98	−0.34	1997–2000	Palestine, Tex.
PLTC	−104.7, 40.2	1.60, 20.50	0.22, 6.25	99	0.85	1996–2000	Platteville, Colo.
PRCO	−97.5, 35.0	0.71, 13.75	0.10, 2.25	97	−0.11	1996–2000	Purcell, Okla.
RWDN	−100.7, 40.1	1.03, 20.00	0.36, 0.75	97	−0.91	1999–2000	McCook, Nebr.
SAV1	−81.7, 32.1	1.49, 17.75	0.21, 11.50	96	−0.58	1999–2000	Savannah, Ga.
SEAW	−122.3, 47.7	0.22, 2.75	0.11, 4.25	73	0.50	1998–2000	Seattle, Wash.
SHK1	−74.0, 40.5	1.17, 20.00	0.25, 2.00	99	−0.68	1998–2000	Sandy Hook, N. J.
SIO3	−117.3, 32.9	0.34, 5.00	0.02, 5.75	86	−0.15	1998–2000	Scripps Pier, San Diego, Calif.
SLAI	−93.7, 41.9	0.65, 19.00	0.21, 10.50	93	−0.81	1999–2000	Slater, Iowa
SYCN	−76.1, 43.1	0.81, 17.00	0.50, 2.25	92	−1.58	1999–2000	Syracuse, N. Y.
TCUN	−103.6, 35.1	0.80, 23.00	0.17, 11.25	99	−0.46	1997–2000	Tucumcari, N. M.
TLKA	−150.4, 62.3	0.18, 2.50	0.79, 10.25	79	−2.23	1998–2000	Talkeetna, Alaska
VCIO	−99.2, 36.1	0.43, 17.25	0.13, 1.25	97	−0.19	1996–2000	Vici, Okla.
WDLM	−95.4, 44.7	1.17, 18.00	0.16, 0.25	97	−0.59	1999–2000	Wood Lake, Minn.
WHN1	−103.3, 42.7	0.69, 21.75	0.43, 11.50	71	−1.32	1999–2000	Whitney, Nebr.
WLCI	−87.1, 40.8	0.88, 18.50	0.19, 0.00	98	−0.53	1999–2000	Wolcott, Indiana
WNCI	−90.5, 39.7	1.00, 16.25	0.51, 10.75	93	−1.15	1999–2000	Winchester, Ill.
WNFL	−92.8, 31.9	1.01, 15.75	0.37, 1.25	97	−0.90	1997–2000	Winnfield, La.
WSMN	−106.3, 32.4	0.33, 0.00	0.08, 8.00	94	0.14	1996–2000	White Sands, N. M.

[a] Stn, station; Lon, longitude; Lat, latitude; A1, amplitude (mm), and P1, phase (local solar time at the maximum), of the diurnal harmonic; A2, amplitude, and P2, phase, of the semidiurnal harmonic of the mean June–August precipitable water; Var, percentage subdaily variance explained by the diurnal and semidiurnal harmonics; Err, percentage sampling error for twice (0000 and 1200 UTC) per day sampling; DP, data period. Both Var and Err are also for June–August season.

the phase in terms of T_{max}, the LST (in hours) at the first maximum of S_n. It can be easily shown that $\sigma_n = \pi/2 - 2\pi n T_{max} n/24$.

[12] Some examples of the fitted diurnal (S_1) and semidiurnal (S_2) harmonics of the PW are shown in Figure 1. It can be seen that the S_1 and S_2 together can represent the diurnal variations very well. In general, the S_1 is the dominant cycle at most of the stations (Figure 1). Figure 2 shows that the S_1 explains over 50% of the subdaily variance, whereas the S_2 accounts for $\leq$25% of the variance (except for the Alaska sites, where the S_2 predominates in June–August (JJA)) (Figure 2). Together, the S_1 and S_2 explain over 80% of the mean subdaily variance at most of the stations (Table 1). We will therefore focus only on these two harmonics.

3. Results

3.1. Validation of the GPS-Sensed PW

[13] There have been a number of validation studies (see section 1 for references) on GPS-sensed PW. The seasonal and spatial variations of our GPS-sensed mean PW (Figures 8e–8h) are in good agreement (spatial correlation of ~0.96) with those derived

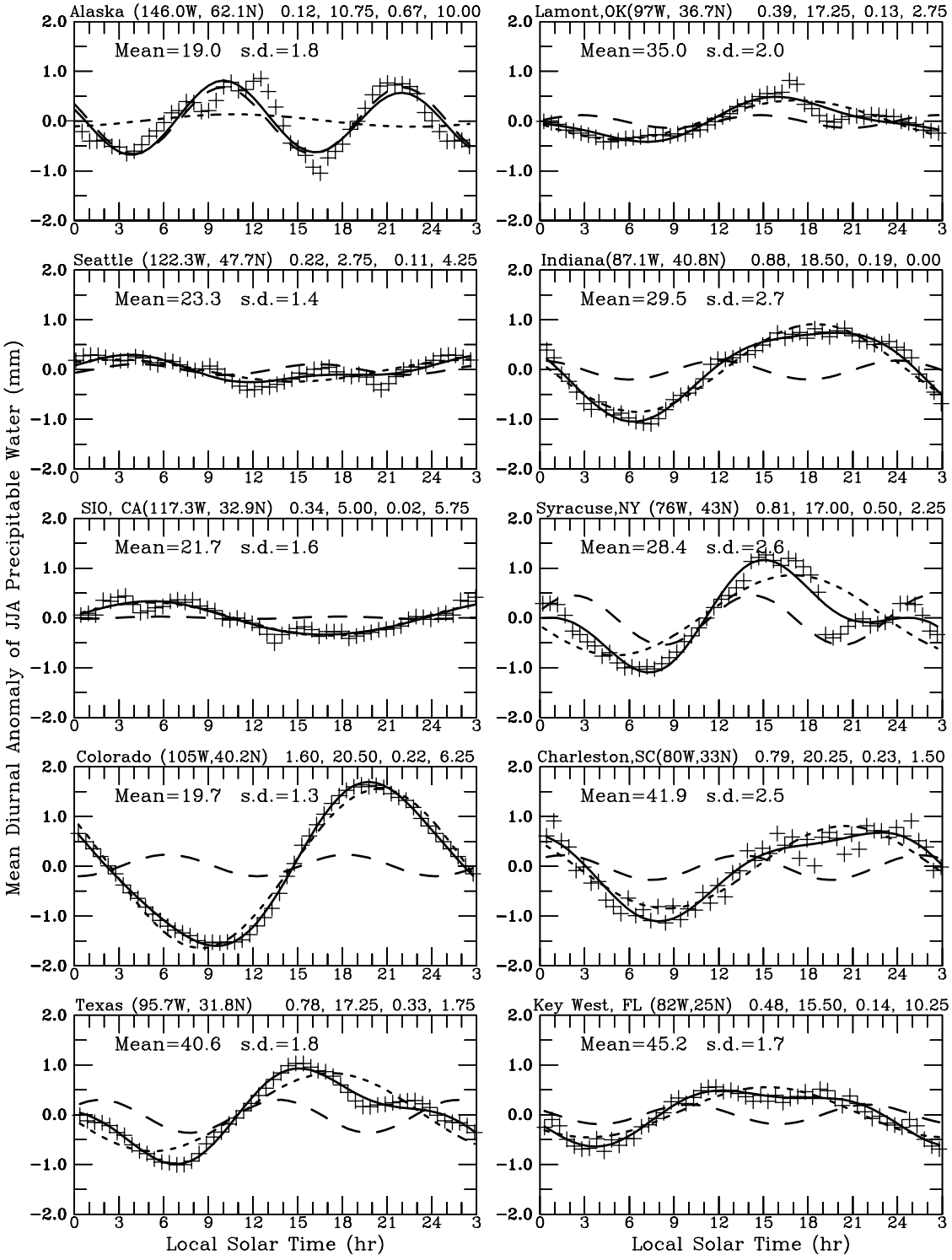

Figure 1. Mean June–August diurnal variations of GPS-sensed precipitable water (PW, pluses) and the fitted diurnal (S_1, short-dashed curve) and semidiurnal (S_2, long-dashed curve) harmonics at 10 GPS stations in North America. Solid curve is $S_1 + S_2$. Mean is the daily mean value (mm), and s.d. (mm) is the mean standard deviation of the day-to-day variation of the diurnal anomalies. Four numbers on top of each panel are, from left to right, the amplitude (mm) and phase (T_{max} in local solar time (LST)) of the S_1 and S_2.

from the NVAP data set [*Randel et al.*, 1996] (not shown). This result provides further evidence that the GPS-sensed PW is reliable and can be applied in climate studies.

[14] The previous validations have not, however, examined the diurnal variations. Here we present a comparison of the PW data for the ARM/CART site near Lamont, Oklahoma, where high-resolution PW observations from GPS, MWR, and radiosonde are available during several intensive operational periods.

[15] Figure 3 compares the individual PW measurements made using the three instruments during July 1997 and January 1998. It

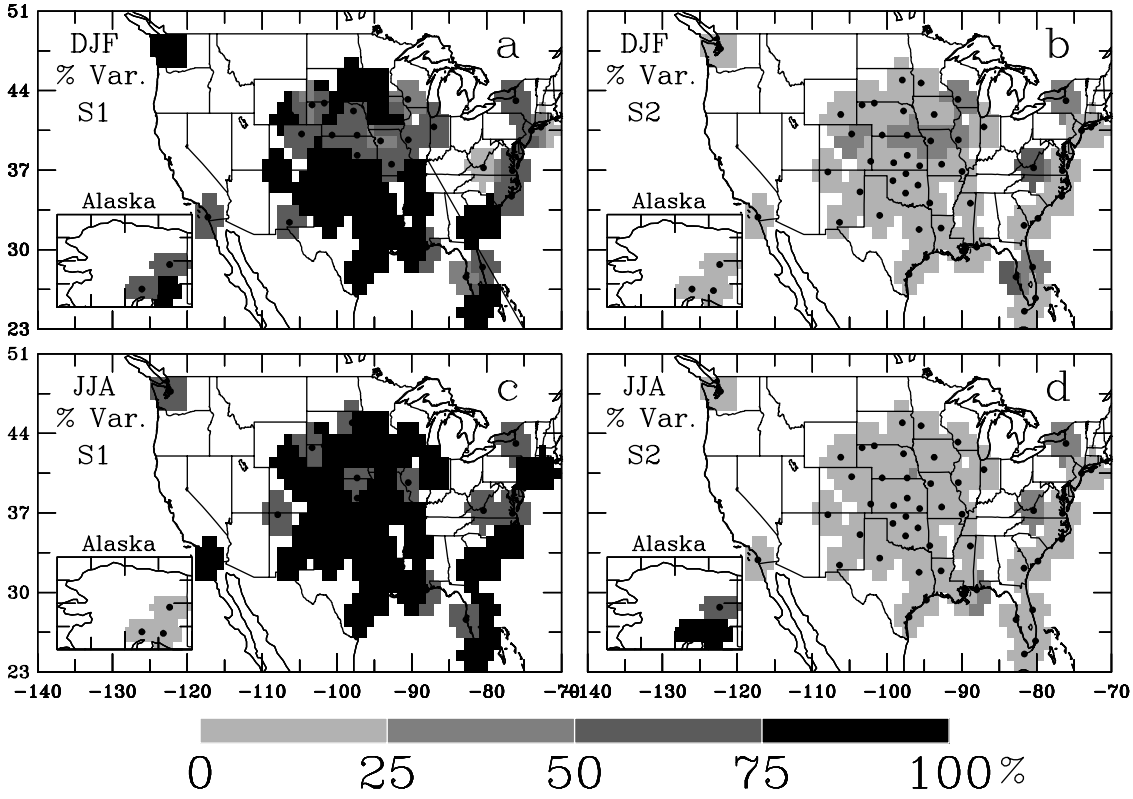

Figure 2. Spatial distribution of percentage subdaily variance explained by the diurnal (left) and semidiurnal (right) harmonics for December–February (top) and June–August (bottom). Dots are the 54 stations listed in Table 1.

can be seen that the GPS method underestimates the PW by ~4–5% (mostly during humid summertime conditions) compared with the MWR and sounding data. A negative bias of GPS-sensed PW was also reported by *Rocken et al.* [1993], *Tregoning et al.* [1998], *Lijegren et al.* [1999] and *Ohtani and Naito* [2000]. *Lijegren et al.* [1999] found that the dry bias can be reduced substantially by lowering the minimum elevation angle from 15° to 7° and by estimating T_m using sounding data. Since we already used a small minimum elevation angle (7°), this dry bias results primarily from errors in T_m. Because T_m is a multiplicative factor (see ((A8)) in Appendix A), the dry bias increases with PW (and thus is larger during wet days).

[16] On the other hand, the MWR and radiosonde observations also differ by a few percentage points (Figure 3c), which could partly result from slight differences in atmospheric locations that were actually measured by the instruments (that is, the MWR and the soundings did not measure the same air mass). This spatial sampling issue is also likely to have contributed to the apparent error of the GPS PW shown in Figure 3a–3b. In general, however, these three measurements of PW are highly correlated with each other ($r > 0.99$). This result suggests that the GPS-sensed PW data are suitable for studying the temporal variations (including the diurnal variations).

[17] To further examine the diurnal variations in these PW observations, we averaged the PW data at each observation time over all the days during each intensive operational period. Figure 4 shows the mean diurnal variations (with the daily mean removed) observed by the three instruments during April 1997, 23 June through 16 July 1997, and 16 September through 10 October 1997. Because the data were averaged over only a relatively small number (20–25) of days, the diurnal signal in Figure 4 is noisy, especially during the spring and autumn months, when the signal is relatively weak. Nevertheless, the GPS, MWR, and radiosonde observations all show significant diurnal variations at the ARM/CART site near Lamont, Oklahoma. Furthermore, the diurnal variations measured by GPS, MWR, and radiosonde agree with each other in general, especially during the summer months, when the diurnal variations are relatively large. This result suggests that the GPS data correctly capture the diurnal variations of PW, even if the diurnal signal is relatively weak (e.g., with a diurnal amplitude ≤0.5 mm). The dry bias in GPS-sensed PW shown in Figure 3 has only minor effects on the mean diurnal variations derived from the GPS data.

3.2. Diurnal Cycle

[18] Figure 5 shows the mean amplitude (i.e., A_1 in equation (2)) and phase (T_{max}) of the diurnal cycle (S_1) derived from the GPS PW data. It can be seen that over the central and eastern United States the amplitude of S_1 is much larger in JJA (~0.5–1.8 mm) than in other seasons. The diurnal amplitude is smallest (0.1–0.8 mm) during March–May (MAM) at most of the stations. Over the southeast the diurnal amplitude is also large (0.5–1.4 mm) during December–February (DJF). The S_1 at the Alaska, Seattle, and San Diego stations is relatively weak (with an amplitude of ≤0.5 mm). The seasonal variation of the diurnal amplitude is strongest over the central United States.

[19] The seasonal minimum of the diurnal amplitude in MAM over the central United States (especially over Kansas and Oklahoma) (Figure 5b) is out of phase with the seasonal minimum of PW in DJF (compare Figures 8e–8h). Even during JJA the S_1 is relatively weak over Kansas and Oklahoma compared with the surrounding regions (Figure 5c). As shown in section 3.3 (Figures 6a–6d), the semidiurnal cycle is also weak over these two states.

[20] The diurnal cycle peaks around noon (1000–1400 LST) in DJF and from midafternoon (mostly in the central United States) to midnight (over New Mexico, Colorado, and Wyoming) in JJA at most of the stations (Figures 5e–5g). During September–Novem-

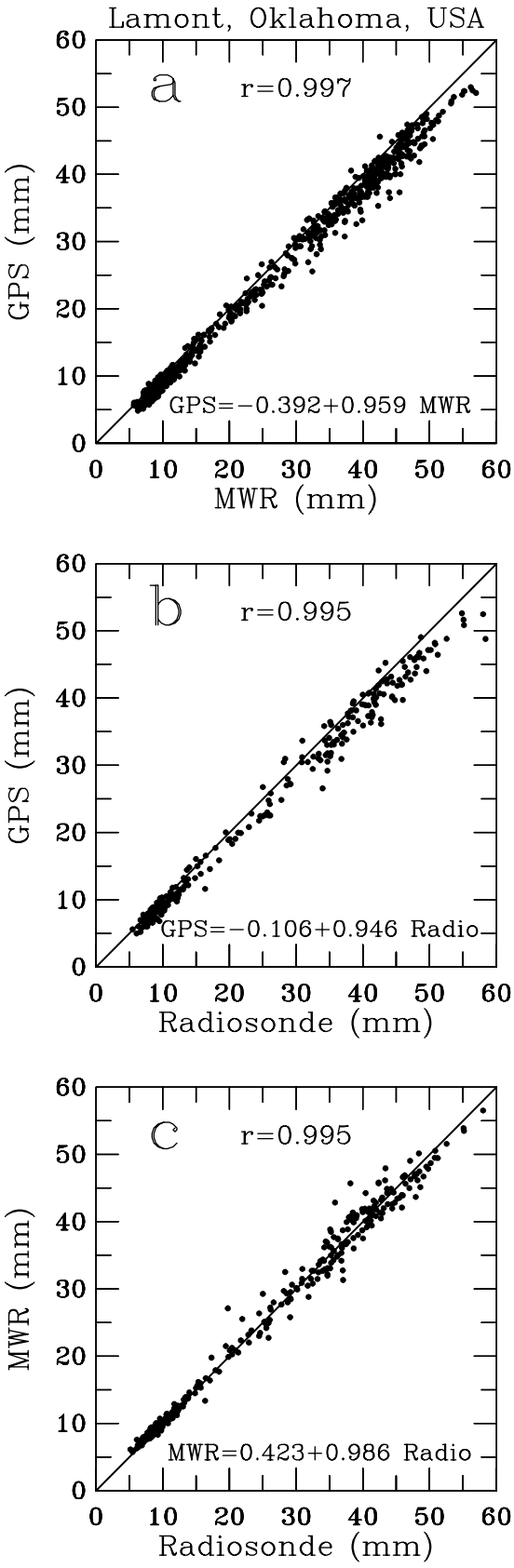

Figure 3. Scatterplots of atmospheric PW (mm) derived from GPS, microwave radiometer (MWR), and radiosondes at the Atmospheric Radiation Measurement Program Cloud and Radiation Testbed (ARM/CART) site in Lamont, Oklahoma, for July 1997 and January 1998. The r is a correlation coefficient of the data points.

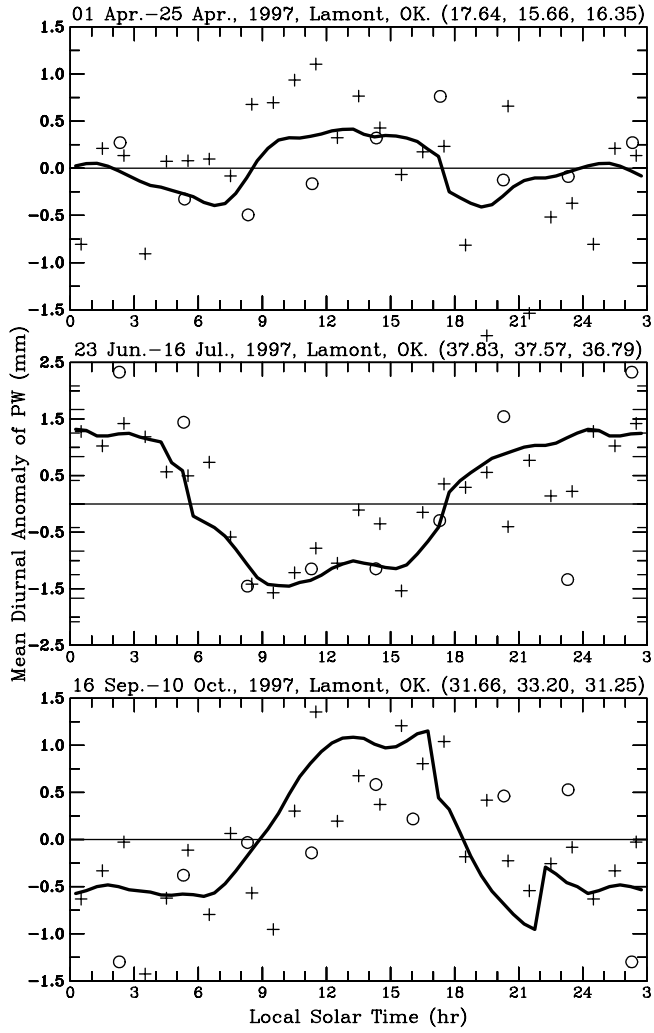

Figure 4. Mean diurnal anomalies of atmospheric PW at the ARM/CART site near Lamont, Oklahoma (97.5°W, 36.7°N), during three periods when 3-hourly radiosonde (circles), hourly microwave radiometer (pluses), and 30-min GPS (solid curves) measurements of PW are all available. Mean standard deviation of the day-to-day variation of the GPS PW diurnal anomalies is ∼1.0, 1.5, and 1.2 mm for the top, middle, and bottom panels, respectively.

ber (SON) the phase pattern of S_1 is similar to that of JJA except that the T_{max} is generally a couple of hours earlier (Figure 5h). In spring the phase pattern (Figure 5f) is noisier than the other seasons, with the T_{max} being around noon in the Midwest and in the late evening over eastern Colorado, Kansas, and Oklahoma (note that the S_1 is weak over these regions (Figure 5b)).

3.3. Semidiurnal Cycle

[21] Figure 6 shows the mean amplitude and phase (T_{max}) of the semidiurnal cycle (S_2) derived from the GPS PW data. In general, the S_2 is much weaker than the S_1 (consistent with Figure 2), with an amplitude of typically about a few tenths of 1 mm. One exception is the Alaska sites, where the S_2 is larger than the S_1 in JJA and MAM (compare Figure 1, top left panel).

[22] The phase of the S_2 is noisier than that of the S_1. In general, the S_2 peaks in early morning and afternoon (for the second cycle) (0200–0400 and 1400–1600 LST) (especially in MAM, Figure 6f) or around midnight and noon (Figures 6e–6g). In particular, the S_2 tends to peak around 0200–0400 (and 1499–1600) LST over

Kansas and Oklahoma in all seasons. During JJA the S_2 peaks around late morning and late evening (1000–1200 and 2200–2400 LST) over Florida, New Mexico, Colorado, and Wyoming (Figure 6g). The S_2 at the Alaska sites peaks in late morning and late evening in all seasons.

3.4. Vertical Structures of Diurnal Variations of Water Vapor

[23] Three-hourly sounding data of atmospheric humidity from the ARM/CART site obtained during the 1994–2000 period were analyzed to obtain the mean diurnal cycle of water vapor in the atmosphere up to 16 km height. Figure 7 shows the seasonal mean diurnal anomalies (divided by standard deviation of the daily mean at each level) of specific humidity (q) from the surface to 16 km in altitude. The number of days used in the averaging is not very large, and thus noise levels in Figure 7 are relatively high. Nevertheless, Figure 7 appears to show a number of interesting features. For example, atmospheric specific humidity above ~2 km is significantly higher from about midnight to 0800 LST than during the day (~0800–1800 LST) in all seasons (the exact timing varies slightly with season). The diurnal cycle varies little from ~4–6 to 16 km above the ground (the diurnal pattern extends up to 20 km, although the humidity sounding data at such altitudes may be unreliable). Near the surface, specific humidity is lower in the morning than in the afternoon and evening in all seasons except summer. This near-surface diurnal cycle propagates upward through the lower troposphere (up to ~4 km). During winter, diurnal anomalies at 4–8 km seem to propagate downward (Figure 7a).

[24] The diurnal phase of GPS-derived PW (Figure 5) at the Lamont site is consistent with that of the radiosonde-measured water vapor in the lower (1–2 km) troposphere (Figure 7) within the sampling error range (<3 hours for the sounding data). For example, the JJA PW peaks around 1700–1800 LST (Figures 5g and 9), while the 1- to 2-km q for JJA has a maximum around 1900–2000 LST (Figure 7c).

[25] It is suggested that the wetting of the Vaisala RS80 sonde (which was used for the ARM observations) in clouds or precipitation may cause a moist bias at higher levels [*Lorenc et al.*, 1996]. In most cases, the sonde sensors should, however, recover quickly after exiting a cloud or precipitation layer by evaporation, causing a moist bias only right above the cloud or rain layer. Our tests showed that including only nonprecipitating days in the q averaging yielded diurnal patterns similar to Figure 7. This suggests that the wetting effect is likely to be small.

3.5. Diurnal Sampling Errors in Radiosonde Humidity

[26] The above results (Figures 1, 5, and 7) show that atmospheric water vapor has significant diurnal variations. These diurnal variations could induce nonnegligible sampling errors if observations are made only a few times per day. The diurnal sampling errors are in addition to the sampling errors due to the existence of days without observations in monthly mean fields discussed by *Kidson and Trenberth* [1988]. Synoptic soundings that were launched around 0000 and 1200 UTC have been the major source of data for atmospheric reanalysis and assimilation data sets and for monthly mean climatology of atmospheric water vapor. To estimate the diurnal sampling errors in these synoptic soundings (and thus in all derived data sets), we sampled the 30-min GPS PW data at 0000 and 1200 UTC and compared the seasonal means derived from the sampled and the original 30-min GPS PW data. The difference between them (expressed as a percentage of the seasonal mean) is shown in Figure 8, together with the seasonal mean PW (from the 30-min GPS data) for each season.

[27] It can be seen that during winter the sampling by the synoptic soundings underestimates the seasonal mean PW by ~1.5–3.0% over much of the eastern coastal United States and the northern Great Plains and overestimates the mean PW by ~0.6–2.0% over the southern Great Plains. The errors at the Seattle and San Diego sites suggest a positive bias of 1.0–2.5% over the western coastal United States during winter. The sampling error is a negative bias over most of the United States in summer and autumn, although the percentage error is generally smaller than those in winter (mainly because the mean PW is larger in summer and autumn) (Figure 8). During spring the sampling error is a positive bias over most of the central United States, whereas it is a negative bias (~1.5%) around the northern coasts of the Gulf of Mexico (Figure 8).

[28] In general, the magnitude of the diurnal sampling errors is small (within ±3% or ±0.5 mm for PW), although these errors are systematic biases (that is, they will not be smoothed out by averaging over time). Increasing the number of samples per day from 2 to 4 (at 0000, 0600, 1200, and 1800 UTC) reduces the sampling error to within about ±1% (not shown). This result suggests that four soundings per day are usually sufficient for sampling seasonal mean PW.

[29] Recently, there have been discussions about rescheduling radiosonde launches according to synoptic conditions for the future configuration of the North American Atmospheric Observing System [*Schlatter*, 1998]. This change could lead to fewer than two launches per day at some stations in order to balance the cost of extra launches at other stations. *Elliott and Ross* [2000] have estimated the biases in long-term monthly mean tropospheric temperature and humidity resulting from this change. Reducing the number of launches per day will obviously increase the diurnal sampling error. For example, we found (not shown) that the diurnal sampling error can easily reach 5–10% at many stations in North America if there is only one randomly scheduled launch per day. The sampling error is similar to that for the current synoptic schedule (Figures 8a–8d) if there are two randomly scheduled (but at least 1 hour apart) launches per day.

4. Discussion on the Causes of Diurnal Variations of Water Vapor

[30] There are many processes that can induce diurnal variations in atmospheric water vapor. These include (1) surface evapotranspiration, which peaks around noon [*Dai et al.*, 1999b]; (2) atmospheric large-scale vertical motion, which tends to be downward from late morning to afternoon and upward from midnight to early morning in the central United States [*Dai et al.*, 1999a]; (3) atmospheric low-level moisture convergence and precipitation, which occurs more frequently around midnight over Kansas and Oklahoma in summer [*Dai et al.*, 1999a]; and (4) vertical mixing (which affects the vertical distribution of water vapor but does not affect the PW) in the planetary boundary layer (the lowest 1–2 km), which is more unstable in the afternoon.

[31] Within the free troposphere (i.e., above 1–2 km) the above-mentioned diurnal cycle of the large-scale vertical motion should induce dry anomalies during the day and wet anomalies at night, which are consistent with the broad pattern shown in Figure 7. Within the lowest 1–2 km, surface evapotranspiration during the day accumulates water vapor and latent heat in the boundary layer before convection breaks out. This is consistent with the peak near-surface specific humidity in the afternoon and early evening in all seasons except summer. During summer, surface moisture convergence and precipitation in Kansas and Oklahoma occur more frequently from late evening to early morning (which is related to the diurnal cycle of large-scale vertical motion [see *Dai et al.*, 1999a]). The summer positive anomalies of near-surface specific humidity (Figure 7c) at night are consistent with the nocturnal precipitation maximum since precipitation can moisten the near-surface air through evaporation. During the other seasons the diurnal cycle of precipitation is weak over this region [*Dai et al.*, 1999a]; thus this moistening effect is small.

[32] Atmospheric PW largely concentrates in the lowest 1–2 km. Therefore all the above processes (except vertical mixing) affecting water vapor in the boundary layer can induce PW diurnal

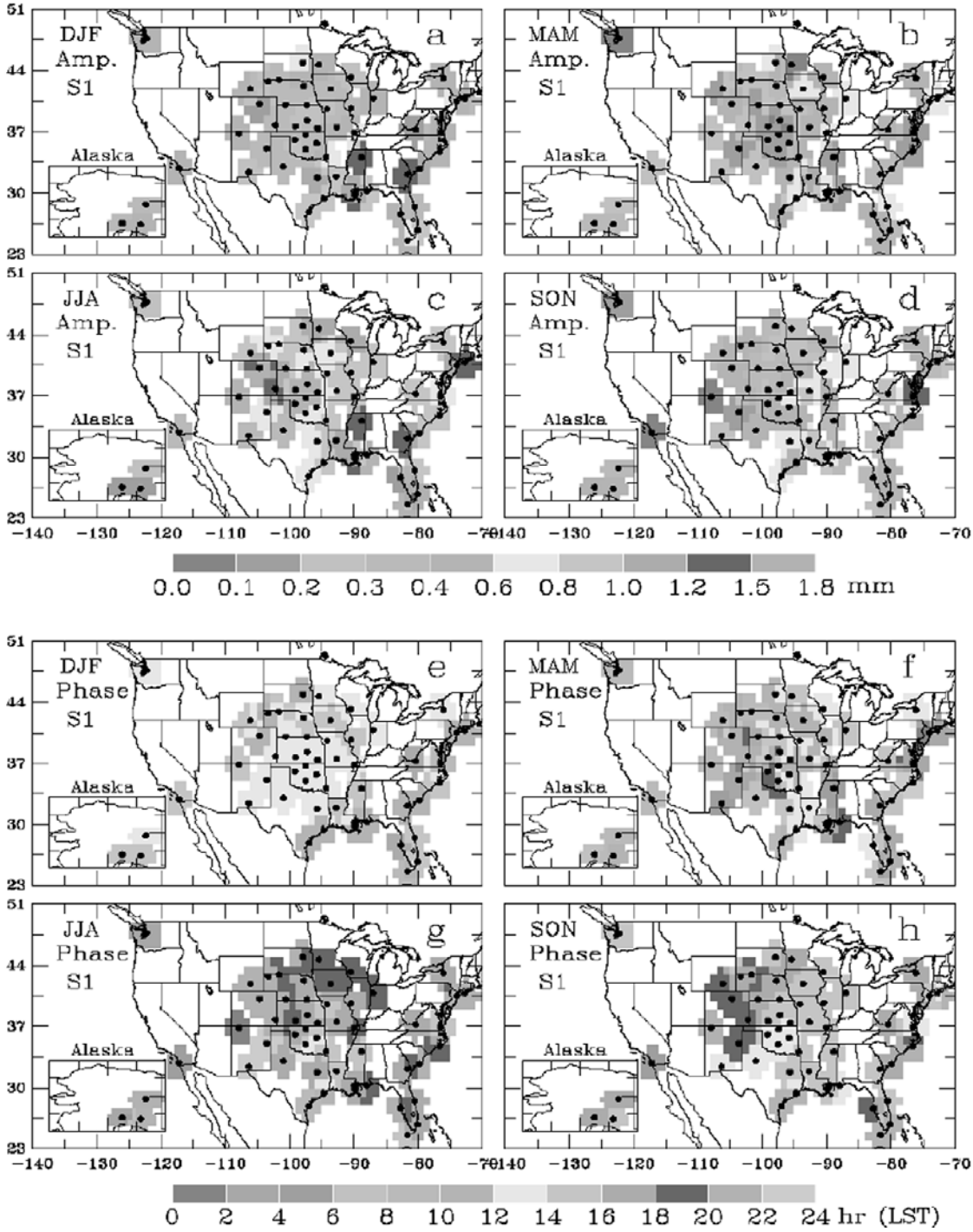

Figure 5. Spatial distribution of the (a–d) amplitude (mm) and (e–h) phase (LST at the maximum) of the diurnal harmonic of seasonal mean PW. See color version of this figure at back of this issue.

variations. In addition, diurnal changes in wind direction (especially in coastal areas) can induce diurnal variations in water vapor and PW. This effect arises because an air mass from the south or the sea usually contains more water than one from the north or inland.

[33] To investigate the relationship between diurnal variations in PW and precipitation, we compare the mean diurnal evolution of GPS-derived PW and precipitation (from hourly rain gauge records of 1963–1993 [*Higgins et al.*, 1996]) at 10 different sites (Figure 9). It can be seen that during summer, higher PW is associated with higher precipitation during the day (often in the afternoon) at some of the sites (e.g., Okolona, Mississippi; Platteville, Colorado; Palestine, Texas; and Key West, Florida). This positive correlation is expected, since precipitation provides a source of water vapor through evaporation within the lower troposphere and on the ground (the water source for precipitation is usually provided through low-level moisture convergence).

[34] Figure 9 also shows weak or little correlation between diurnal variations of PW and precipitation at a number of sites (e.g., SIO, California; Lamont, Oklahoma; Wolcott, Indiana; and Charleston, South Carolina). Some of these sites are located in coastal areas, and the diurnal cycle of PW is likely to be affected

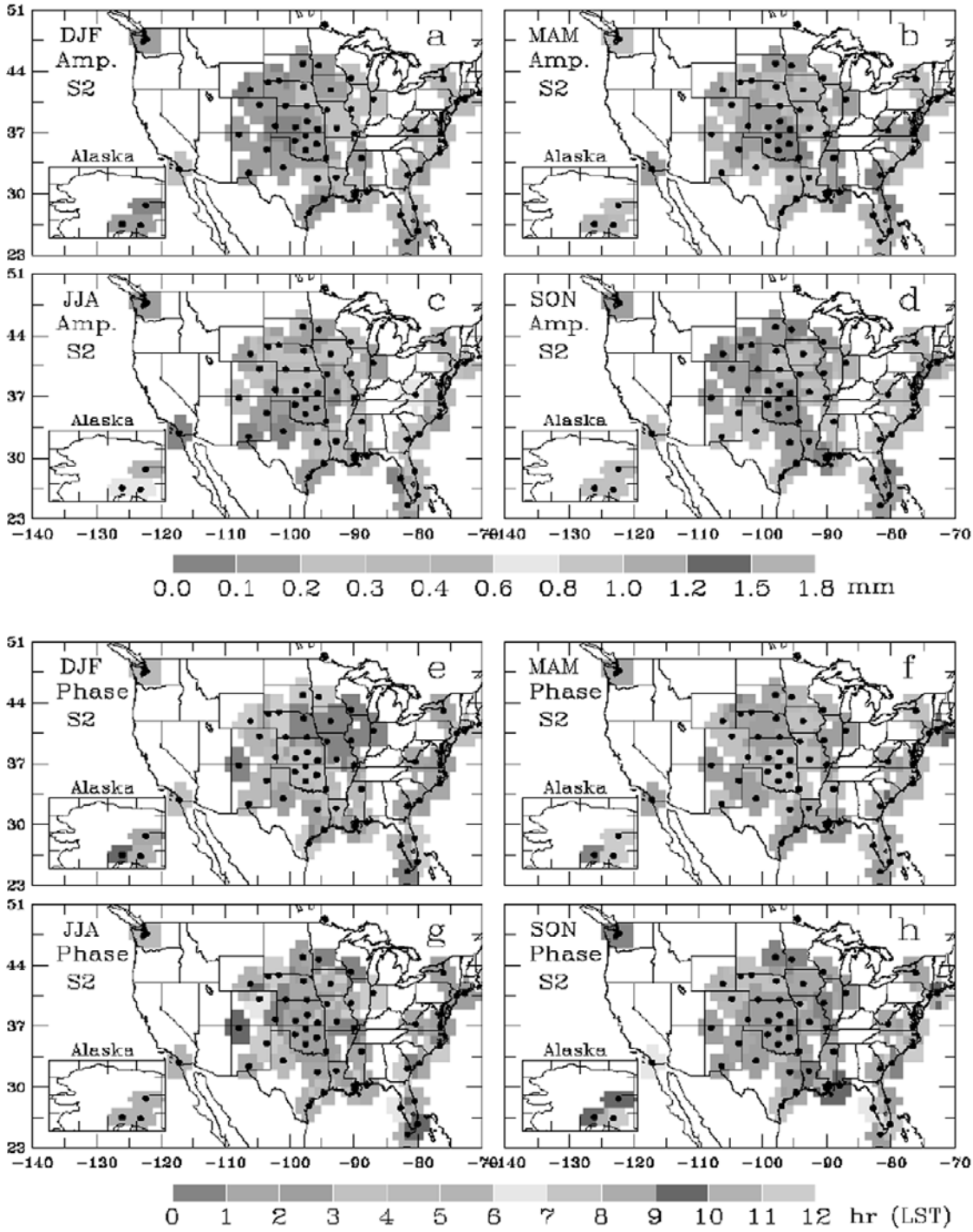

Figure 6. Same as in Figure 5 but for the semidiurnal harmonic. Phase is LST at the first maximum. See color version of this figure at back of this issue.

by changes in wind direction (e.g., the sea breeze circulation). At the Lamont, Oklahoma, site the midnight to early morning maximum of precipitation is associated with positive water vapor anomalies within the lowest ~0.6 km, whereas the late afternoon (around 1700–1800 LST) maximum of PW results from peak humidity within the 0.5- to 2.0-km layer (Figures 7 and 9). This result suggests that the PW diurnal cycle can be out of phase with the diurnal variations of near-surface water vapor and precipitation.

[35] During winter, positive correlation between the diurnal variations of PW and precipitation was found at some of the sites (e.g., Seattle, Washington; Palestine, Texas; and Charleston, South Carolina) (not shown). Since precipitation has only a weak diurnal cycle during the cold season [*Dai et al.*, 1999a], its effect (through evaporation) on the diurnal cycle of PW is likely to be limited.

5. Summary

[36] To study the diurnal variations in atmospheric water vapor, we analyzed 30-min-averaged data of atmospheric precipitable water (PW) derived using GPS path delay data of the 1996–2000 period from 54 stations in North America. The GPS PW

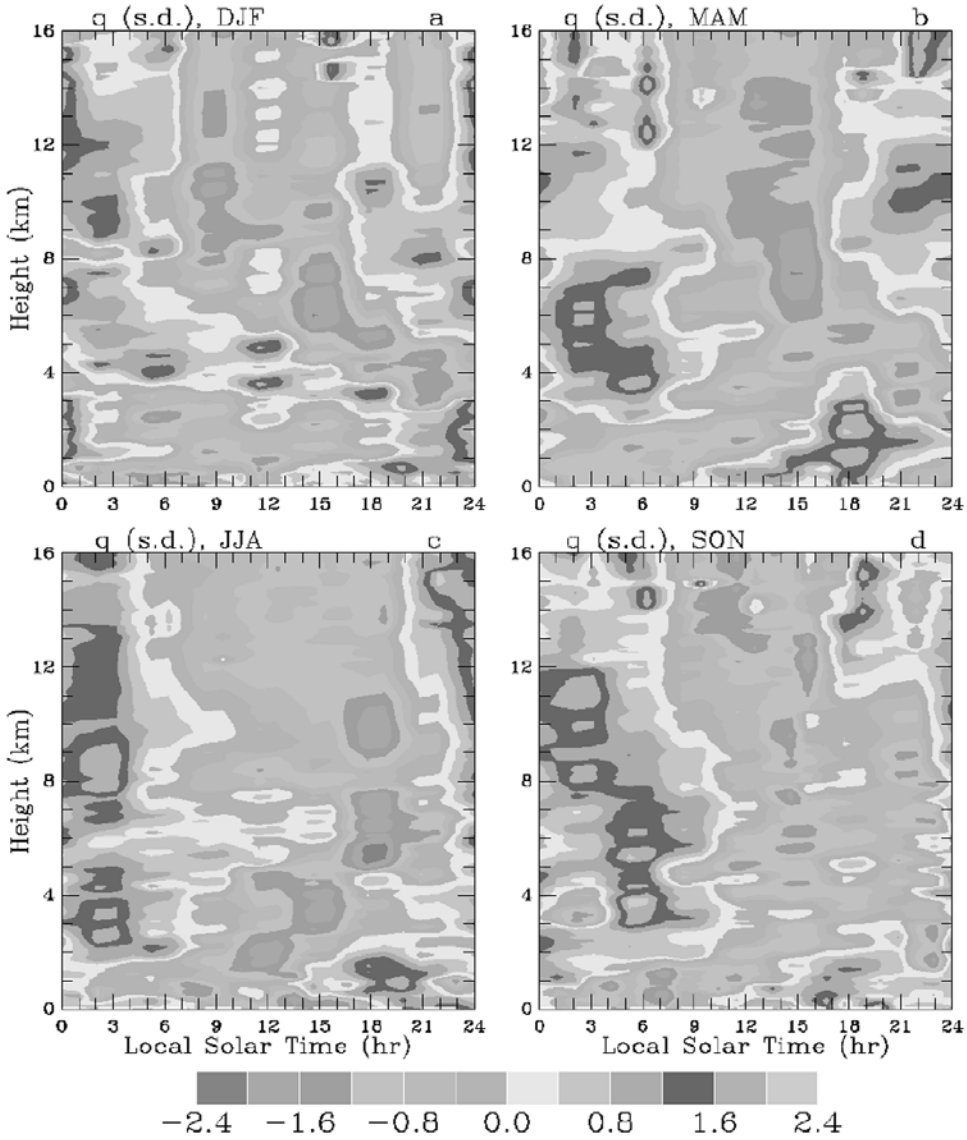

Figure 7. Seasonal mean diurnal anomalies (normalized by the standard deviation of the daily mean at each level) of atmospheric specific humidity derived from 3-hourly radiosonde data for 1994–2000 at the ARM/CART site near Lamont, Oklahoma. Number of days with eight soundings per day included in the averaging is 38 for DJF, 93 for MAM, 86 for JJA, and 92 for SON. Standard deviation of the daily mean for JJA ranges from ~0.50 g kg^{-1} at the surface to 0.76 g kg^{-1} around 1 km and <0.10 g kg^{-1} above 5.5 km. See color version of this figure at back of this issue.

observations from Lamont, Oklahoma, were compared with high-resolution radiosonde and ground-based microwave radiometer (MWR) observations of PW. The seasonal mean profiles (up to 16 km height) of the diurnal anomalies of atmospheric specific humidity at Lamont, Oklahoma, were also examined using 3-hourly radiosonde data from the ARM/CART site obtained during the 1994–2000 period. The diurnal sampling errors in seasonal mean PW derived from synoptic soundings (at 0000 and 1200 UTC) were estimated by sampling the 30-min GPS data and comparing the mean PW derived from the sampled and the original PW data. The following is a summary of the main findings.

[37] The seasonal and spatial variations of the GPS mean PW are in good agreement with those derived from other PW data sets (e.g., NVAP). The 30-min GPS PW data were highly correlated ($r > 0.99$) with the radiosonde and MWR measurements from the ARM/CART site. The mean diurnal variations derived from the GPS PW data agree with those derived from the sounding and MWR data at Lamont, Oklahoma. On the other hand, the GPS method tends to underestimate the PW by ~4–5% (most pronounced during humid days) at the Lamont site compared with sounding and MWR data. This bias, however, has little effect on our diurnal results.

[38] Significant diurnal variations of PW were found at most of the 54 GPS stations. The diurnal (24 hour) cycle, S_1, which explains over 50% of the subdaily variance, has an amplitude of 1.0–1.8 mm over most of the central and eastern United States during summer. The diurnal amplitude is smaller ($\leq$0.8 mm) in other seasons. The S_1 is weakest in spring over most of the stations. The S_1 generally peaks around noon (1000–1400 LST) in winter and from midafternoon to midnight in summer. The phase of S_1 in autumn is a couple of hours earlier than in summer.

[39] The semidiurnal (12 hour) cycle, S_2, which accounts for <25% of the subdaily variance, is generally weak, with an amplitude of only about a few tenths of 1 mm. One exception is

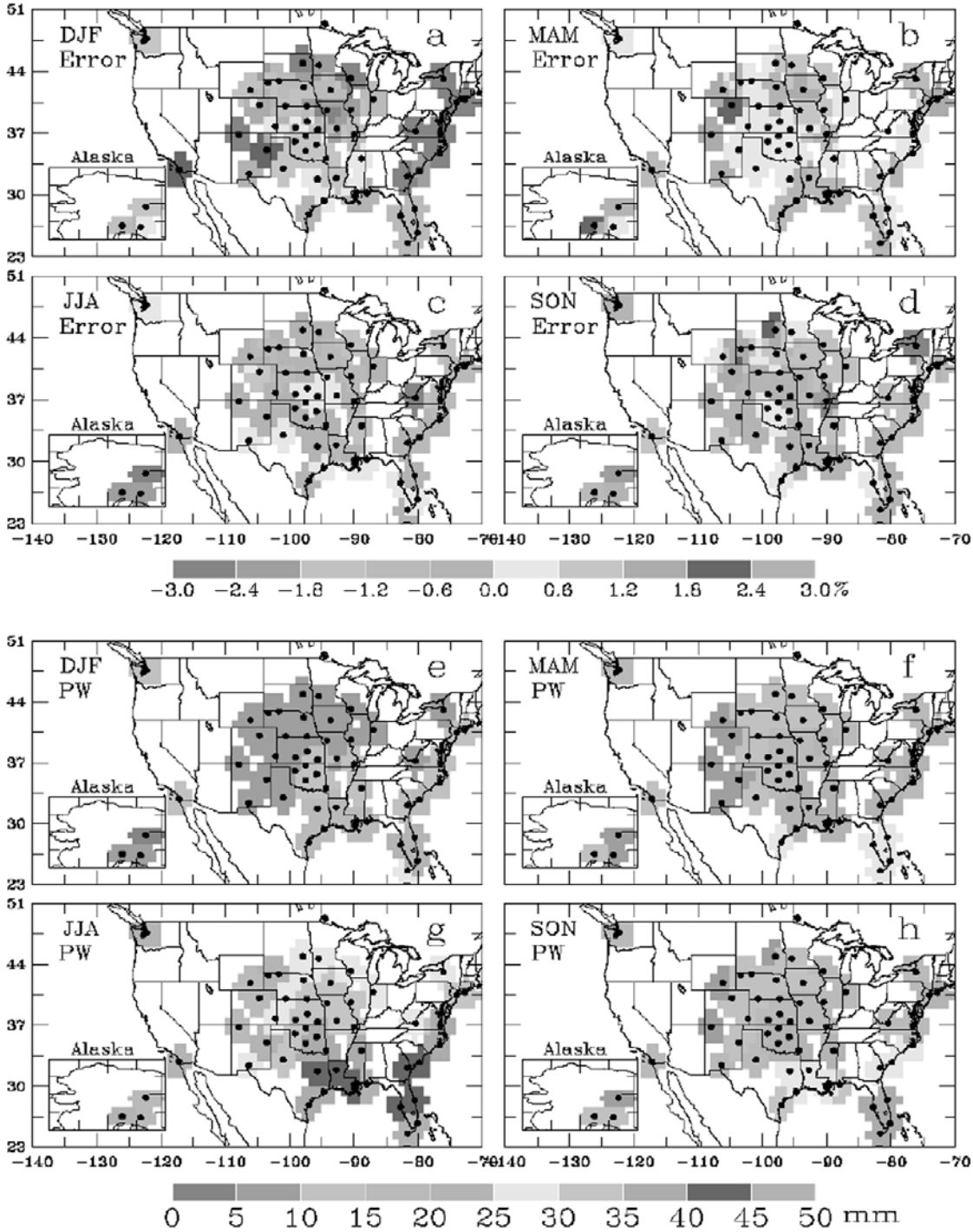

Figure 8. (a–d) Spatial distribution of the diurnal sampling error (percent) for twice (0000 and 1200 UTC) per day sampling and (e–h) seasonal mean PW derived from the 30-min GPS data (mm). See color version of this figure at back of this issue.

the Alaska sites, where the S_2 (~0.5–0.7 mm) is larger than the S_1 in JJA and MAM. In general, the S_2 peaks in early morning and afternoon (0200–0400 and 1400–1600 LST).

[40] The vertical structure of the diurnal variation of specific humidity at Lamont, Oklahoma, is characterized by higher humidity in the early morning (~0000–0800 LST) than during the day (~0800–1800 LST) in the free troposphere and low stratosphere. This diurnal pattern varies little from ~4–6 to 16 km above the ground. In the lower troposphere the humidity diurnal cycle is more complicated. Near the surface, specific humidity tends to be lower in the morning than in the afternoon and evening in all seasons except summer. This near-surface diurnal cycle propagates upward through the lower troposphere (up to ~4 km). It is suggested that upward motion at night and downward motion during the day contribute to the diurnal humidity cycle in the free troposphere and lower stratosphere at Lamont, Oklahoma. Within the lower troposphere, where most of the PW resides, several processes, including surface evapotranspiration, vertical mixing,

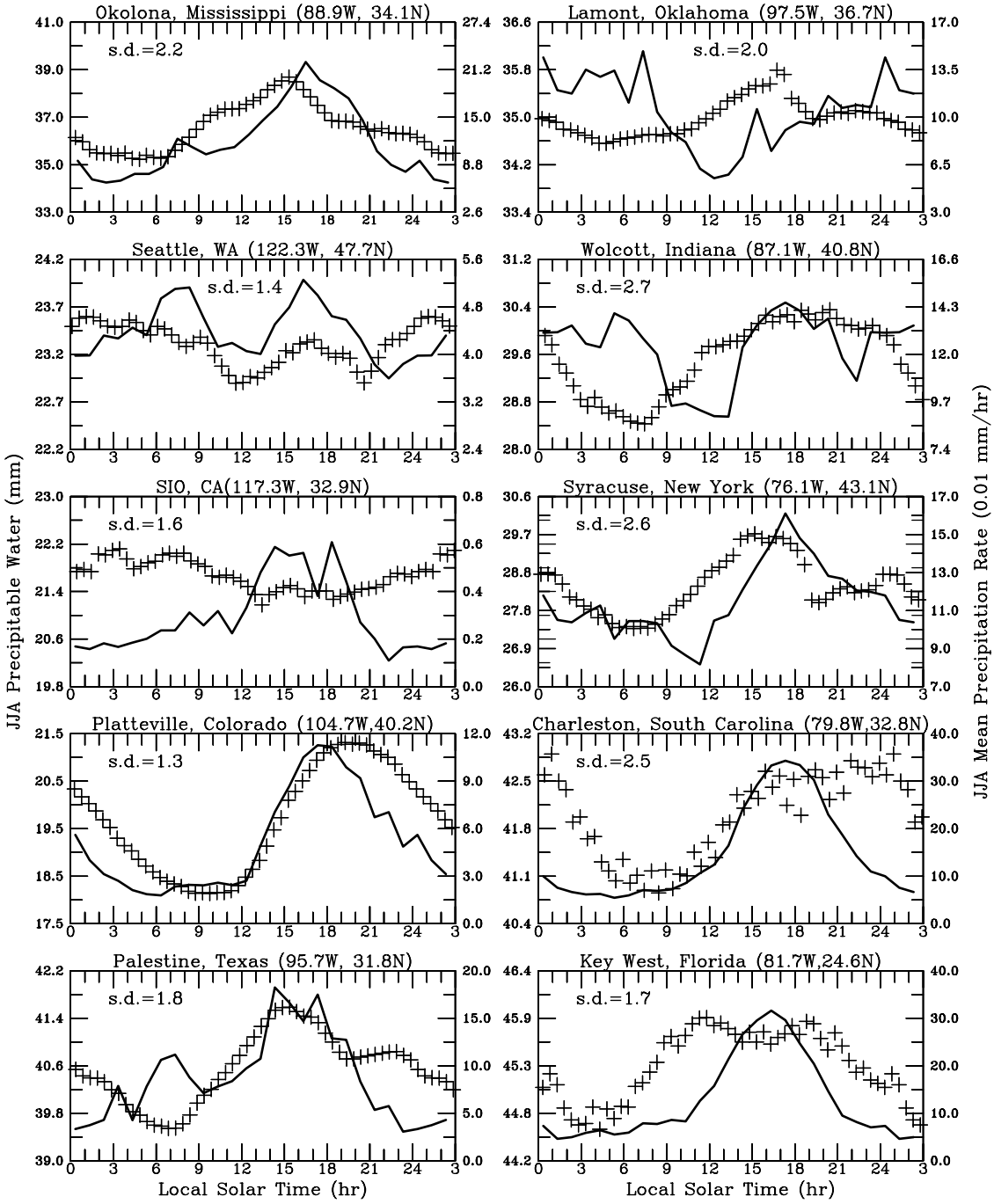

Figure 9. June–August mean diurnal variations of GPS-sensed PW (pluses; read on the left ordinate) and precipitation (solid curve; read on the right ordinate) at 10 GPS stations over the United States. The s.d. is the mean standard deviation (mm) of the day-to-day variation of the PW diurnal anomalies.

low-level moisture convergence, and precipitation, all affect the diurnal variation of water vapor.

[41] The twice-daily sampling (at 0000 and 1200 UTC) by synoptic soundings does not resolve the diurnal variation of humidity and could lead to errors in both monthly and seasonal mean PW. We found that in general, the magnitude of this diurnal sampling error is small (within ±3% of the mean or ±0.5 mm for PW). During winter the sampling by synoptic soundings underestimates seasonal mean PW by ~1.5–3.0% over most of the eastern coastal United States and the northern Great Plains and overestimates the mean PW over the southern Great Plains (by ~0.6–2.0%) and the western coastal United States (by ~1.0–2.5%). The diurnal sampling error is a negative bias over much of the United States in summer and autumn, with a smaller percentage error than for winter. During spring the sampling error is a positive bias over most of the central United States. Reducing the number of radiosonde launches to one launch per day can easily increase the diurnal sampling error to 5–10% in North America.

[42] The results of this study suggest that atmospheric water vapor has significant diurnal variations, although the diurnal amplitude is generally small (≤5% of the mean). Nevertheless, the diurnal signal in atmospheric water vapor is very clear from the surface up to the tropopause at Lamont, Oklahoma. Further analyses for other locations are needed.

Appendix A. GPS Meteorology

[43] The method for deriving atmospheric precipitable water (PW) using GPS data is described in detail by *Bevis et al.* [1992, 1994]. Here we briefly summarize this method and the procedures we used to compute the PW.

[44] The atmosphere affects microwave transmissions from space in two ways. First, the waves travel slower than they would in a vacuum. Second, they travel in a curved path instead of in a straight line because of a variable index of refraction along the ray path. The delay in signal arrival time can be stated in terms of an equivalent increase in travel path length. This excess path length, or total atmospheric delay, is given by [*Bevis et al.*, 1992]

$$\Delta L = \int_L n(s)ds - G = 10^{-6}\int_L N(s)ds + (S - G), \qquad \text{(A1)}$$

where $n(s)$ is the refractive index as a function of position s along the curved ray path L, G is the straight-line geometrical path length through the atmosphere (the path that would occur if the atmosphere were replaced by a vacuum), S is the geometrical path length along L, and $N(s) = 10^6(n(s) - 1)$ is atmospheric refractivity. The first term on the far right-hand side, $10^{-6}\int_L N(s)ds$, is due to the slowing effect, and the second term, (S − G), is due to bending.

[45] The refractivity of the atmosphere is a function of its temperature, pressure, and water vapor pressure. It can be computed (with an accuracy better than 0.5%) using the following formula [*Boudouris*, 1963]:

$$N = k_1\frac{P_d}{T} + k_2\frac{P_v}{T} + k_3\frac{P_v}{T^2}, \qquad \text{(A2)}$$

where P_d and P_v are the partial pressures (in millibars) of dry air and water vapor, respectively; T is the atmospheric temperature (in degrees Kelvin); and k_1, k_2, and k_3 are constants and are given by *Bevis et al.* [1994].

[46] *Saastamoinen* [1972] and *Davis et al.* [1985] showed that the total atmospheric delay, ΔL, which is computed based on the relative locations of the GPS receiver and the GPS satellite using GPS software (e.g., the Bernese GPS software [*Beutler et al.*, 1996]), can be partitioned into a large quantity, ΔL_h, which depends only on surface pressure, called the "hydrostatic delay" or "dry delay," and a smaller quantity, ΔL_w, which is a function of water vapor distribution and is called the "wet delay." The hydrostatic delay in the zenith direction can be computed using [*Elgered et al.*, 1991]

$$\Delta L_h^o = 2.2779 \times 10^{-3}\frac{P_s}{f(\lambda, H)}, \qquad \text{(A3)}$$

where P_s is the total surface pressure in millibars and $f(\lambda, H)$ is a factor for correcting the local gravity,

$$f(\lambda, H) = 1 - 0.00266\cos(2\lambda) - 0.00028H, \qquad \text{(A4)}$$

where λ is the latitude and H is the height of the surface above the ellipsoid (in kilometers). The zenith hydrostatic delay can be converted to ΔL_h using a mapping function $M_h(\alpha)$, where α is the observation elevation angle. We computed ΔL_h using the Saastamoinen model [*Saastamoinen*, 1972] for the years before 2000 and using the dry mapping function of *Niell* [1996] for year 2000.

[47] The wet delay can then be estimated as $\Delta L - \Delta L_h$. The wet delay is normally converted to the wet delay along the zenith path (zenith wet delay (ZWD)) using a mapping function $M_w(\alpha)$,

$$\mathrm{ZWD} = \left(\Delta L - \Delta L_h^o\, M_h(\alpha)\right)/M_w(\alpha). \qquad \text{(A5)}$$

We used $M_w(\alpha)$ of *Niell* [1996],

$$M_w(\alpha) = \left(\frac{1}{1 + \frac{a}{1+\frac{b}{1+c}}}\right)\Bigg/\left(\frac{1}{\sin(\alpha) + \frac{a}{\sin(\alpha)+\frac{b}{\sin(\alpha)+c}}}\right) \qquad \text{(A6)}$$

where parameters a, b, and c are functions (with similar form) of latitude λ and time of the year [see *Niell*, 1996, equation (5)]. Their typical values are listed in Table 4 of *Niell* [1996].

[48] Now, since the ZWD is a function of atmospheric water vapor and temperature [*Elgered et al.*, 1991; *Bevis et al.*, 1992],

$$\mathrm{ZWD} = 10^{-6}\left[k'_2\int\left(\frac{P_v}{T}\right)dz + k_3\int\left(\frac{P_v}{T^2}\right)dz\right], \qquad \text{(A7)}$$

where $k'_2 = k_2 - mk_1$ and m is M_w/M_d, the ratio of the molar masses of water vapor and dry air, this allows PW to be calculated. Using (A7), PW (in millimeters) can be related to ZWD (in millimeters) via [*Bevis et al.*, 1992, 1994],

$$\mathrm{PW} = \pi\mathrm{ZWD}, \qquad \text{(A8)}$$

where π is a dimensionless parameter ($\sim 0.15 \pm 0.02$) and is given by

$$\pi^{-1} = 10^{-6}\rho R_v[(k_3/T_m) + k'_2], \qquad \text{(A9)}$$

where ρ is the density of liquid water, R_v is the specific gas constant for water vapor, and T_m is a weighted mean temperature of the atmosphere [*Davis et al.*, 1985],

$$T_m = \int (P_v/T)dz \Big/ \int (P_v/T^2)dz. \qquad \text{(A10)}$$

[49] It has been shown that T_m can be estimated fairly accurately (with a relative error of <2%) using surface air temperature when atmospheric profiles of temperature and humidity are unavailable [*Bevis et al.*, 1994; *Ross and Rosenfeld*, 1997]. *Bevis et al.* [1994] showed that using 3-D weather forecast fields can reduce this error to <1%.

[50] We used station air temperature (T_s) to estimate T_m using the local $T_m - T_s$ relationship, derived from soundings at Norman, Oklahoma, for stations LMNO, VCIO, PRCO, and HKLO, and using the $T_m - T_s$ relationship derived from soundings in Denver, Colorado, for station PLTC. The $T_m - T_s$ relationship of *Bevis et al.* [1994] was used for all the other stations.

[51] **Acknowledgments.** We are grateful to Hans-Georg Scherneck of Onsala Space Observatory, Sweden, for calculating the leading tidal components of displacement at the GPS sites. We thank Anthony D. Del Genio for sharing his thoughts on processes affecting the diurnal cycle of water vapor. Comments from Kevin Trenberth and two anonymous reviewers have been very helpful. This work was supported by small grants from Jay Fein (NSF) and Rick Lawford (NOAA Office of Global Programs). The sounding data were obtained from the Atmospheric Radiation Measurement (ARM) Program sponsored by the U.S. Department of Energy. NOAA Forecast Systems Laboratory (FSL) provided the GPS tracking data. The National Center for Atmospheric Research is sponsored by the National Science Foundation.

References

Beutler, G., E. Brockmann, S. Fankhauser, W. Gurtner, J. Johnson, L. Mervart, M. Rothacher, S. Schaer, T. Springer, and R. Weber, *Bernese GPS Software Version 4.0 Documentation*, Univ. of Bern, Bern, Switzerland, 1996.

Bevis, M., S. Businger, T. A. Herring, C. Rocken, R. A. Anthes, and R. H. Ware, GPS meteorology: Remote sensing of atmospheric water vapor using the Global Positioning System, *J. Geophys. Res.*, *97*, 15,787–15,801, 1992.

Bevis, M., S. Businger, S. Chiswell, T. A. Herring, R. Anthes, C. Rocken, and R. H. Ware, GPS meteorology: Mapping zenith wet deplays onto precipitable water, *J. Appl. Meteorol.*, *33*, 379–386, 1994.

Boudouris, G., On the index of refraction of air, the absorption and dispersion of centimeter waves by gases, *J. Res. Natl. Bur. Stand., U.S. Sect. D, 67*, 631–684, 1963.

Dai, A., Global precipitation and thunderstorm frequencies, *II, Diurnal variations, J. Clim.*, *14*, 1112–1128, 2001.

Dai, A., and C. Deser, Diurnal and semidiurnal variations in global surface wind and divergence fields, *J. Geophys. Res.*, *104*, 31,109–31,125, 1999.

Dai, A., and J. Wang, Diurnal and semidiurnal tides in global surface pressure fields, *J. Atmos. Sci.*, *56*, 3874–3891, 1999.

Dai, A., F. Giorgi, and K. E. Trenberth, Observed and model-simulated precipitation diurnal cycle over the contiguous United States, *J. Geophys. Res.*, *104*, 6377–6402, 1999a.

Dai, A., K. E. Trenberth, and T. R. Karl, Effects of clouds, soil moisture, precipitation and water vapor on diurnal temperature range, *J. Clim.*, *12*, 2451–2473, 1999b.

Davis, J. L., T. A. Herring, I. I. Shapiro, A. E. E. Rogers, and G. Elgered, Geodesy by radio interferometry: Effects of atmospheric modeling errors on estimates of baseline length, *Radio Sci.*, *20*, 1593–1607, 1985.

Duan, J., et al., GPS meteorology: Direct estimation of the absolute value of precipitable water, *J. Appl. Meteorol.*, *35*, 830–838, 1996.

Elgered, G., J. L. Davis, T. A. Herring, and I. I. Shapiro, Geodesy by radio interferometry: Water vapor radiometry for estimation of the wet delay, *J. Geophys. Res.*, *96*, 6541–6555, 1991.

Elliott, W. P., and R. J. Ross, Estimated impacts on climate records of adaptive strategies for scheduling radiosondes, *J. Clim.*, *13*, 2116–2120, 2000.

Fang, P., M. Bevis, Y. Bock, S. Gutman, and D. Wolfe, GPS meteorology: Reducing systematic errors in geodetic estimates for zenith delay, *Geophys. Res. Lett.*, *25*, 3583–3586, 1998.

Guichard, F., D. Parsons, and E. Miller, Thermodynamic and radiative impact of the correction of sounding humidity bias in the tropics, *J. Clim.*, *13*, 3611–3624, 2000.

Han, Y., and E. Westwater, Remote sensing of tropospheric water vapor and cloud liquid water by integrated ground-based sensors, *J. Atmos. Oceanic Technol.*, *12*, 1050–1059, 1995.

Higgins, R. W., J. E. Janowiak, and Y.-P. Yao, A gridded hourly precipitation database for the United States (1963–1993), *NCEP/Clim. Predict. Cent. Atlas 1*, 47 pp., U.S. Dep. of Comm., Washington, D. C., 1996.

Kidson, J. W., and K. E. Trenberth, Effects of missing data on estimates of monthly mean general circulation statistics, *J. Clim.*, *1*, 1261–1275, 1988.

Leick, A., *GPS Satellite Surveying*, 353 pp., John Wiley, New York, 1990.

Lesht, B. M., Reanalysis of radiosonde data from the 1996 and 1997 water vapor intensive observation periods: Application of the Vaisala RS-80H contamination correction algorithm to dual-sonde soundings, paper presented at the 9th Annual Atmospheric Radiation Measurements (ARM) Science Team Meeting, Dep. of Energy, San Antonia, Tex., 22–26 March 1999.

Lijegren, J., B. Lesht, T. Van Hove, and C. Rocken, A comparison of integrated water vapor from microwave radiometer, balloon-borne sounding system and Global Positioning System, paper presented at the 9th Annual ARM Science Team Meeting, San Antonia, Texas, 22–26 March 1999.

Liou, Y.-A., Y.-T. Teng, T. Van Hove, and J. C. Liljegren, Comparison of precipitable water observations in the near tropics by GPS, microwave radiometer, and radiosondes, *J. Appl. Meteorol.*, *40*, 5–15, 2001.

Lorenc, A. C., D. Barker, R. S. Bell, B. Macpherson, and A. J. Maycock, On the use of radiosonde humidity observations in mid-latitude NWP, *Meteorol. Atmos. Phys.*, *60*, 3–17, 1996.

MacDonald, A., Y. Xie, and R. Ware, Diagnosis of three dimensional water vapor using slant observations from a GPS network, *Mon. Weather Rev.*, *130*, 369–397, 2002.

Niell, A. E., Global mapping functions for the atmospheric delay at radio wavelengths, *J. Geophys. Res.*, *101*, 3227–3246, 1996.

Ohtani, R., and I. Naito, Comparison of GPS-derived precipitable water vapors with radiosonde observations in Japan, *J. Geophys. Res.*, *105*, 26,917–26,929, 2000.

Randel, D. L., T. H. Vonder Haar, M. A. Ringerud, G. L. Stephens, T. J. Greenwald, and C. L. Combs, A new global water vapor dataset, *Bull. Am. Meteorol. Soc.*, *77*, 1233–1246, 1996.

Rocken, C., R. H. Ware, T. Van Hove, F. Solheim, C. Alber, and J. Johnson, Sensing atmospheric water vapor with the Global Positioning System, *Geophys. Res. Lett.*, *20*, 2631–2634, 1993.

Rocken, C., T. Van Hove, and R. Ware, Near real-time GPS sensing of atmospheric water vapor, *Geophys. Res. Lett.*, *24*, 3221–3224, 1997.

Ross, R. J., and S. Rosenfeld, Estimating mean weighted temperature of the atmosphere for Global Positioning System applications, *J. Geophys. Res.*, *102*, 21,719–21,730, 1997.

Saastamoinen, J., Atmospheric correction for the troposphere and stratosphere in radio ranging of satellites, in *The Use of Artificial Satellites for Geodesy, Geophys. Monogr. Ser.*, vol. 15, edited by S. W. Henriksen, A. Mancini, and B. H. Chovitz, pp. 247–251, AGU, Washington, D. C., 1972.

Schlatter, T., Testing hypotheses about atmospheric observing systems for NAOS, in *Proceedings of AMS Symposium on Research Foci of the U.S. Weather Research Program*, Phoenix, AZ, pp. 507–509, 1998.

Solheim, F., J. Godwin, E. Westwater, Y. Han, S. Keihm, K. Marsh, and R. H. Ware, Radiometric profiling of temperature, water vapor, and liquid water using various inversion methods, *Radio Sci.*, *33*, 393–404, 1998.

Tregoning, P., R. Boers, D. O'Brien, and M. Hendy, Accuracy of absolute precipitable water vapor estimates from GPS observations, *J. Geophys. Res.*, *103*, 28,701–28,710, 1998.

Wang, J., W. B. Rossow, and Y. Zhang, Cloud vertical structure and its variations from a 20-yr global rawinsonde dataset, *J. Clim.*, *13*, 3041–3056, 2000.

Wang, J., H. L. Cole, D. J. Carlson, E. R. Miller, K. Beierle, and A. Paukkunen, Corrections of humidity measurement errors from the Vaisala RS80_A radiosonde—Application to TOGA_COARE data, *J. Atmos. Oceanic Technol.*, in press, 2002.

Ware, R. H., C. Alber, C. Rocken, and F. Solheim, Sensing integrated water vapor along GPS ray paths, *Geophys. Res. Lett.*, *24*, 417–420, 1997.

Ware, R. H., D. W. Fulker, S. A. Stein, D. N. Anderson, S. K. Avery, R. D. Clark, K. K. Droegemeier, J. P. Kuettner, J. B. Minster, and S. Sorooshian, SuomiNet: A real-time national GPS network for atmospheric research and education, *Bull. Am. Meteorol. Soc.*, *81*, 677–694, 2000.

A. Dai and J. Wang, Climate and Global Dynamics Division, National Center for Atmospheric Research, P.O. Box 3000, 1850 Table Mesa Drive, Boulder, CO 80307, USA. (adai@ucar.edu; junhong@ucar.edu)

T. Van Hove and R. Ware, GPS Science and Tehcnology Program, University Corporation for Atmospheric Research, P.O. Box 3000, Boulder, CO 80307, USA. (vanhove@ucar.edu; ware@ucar.edu)

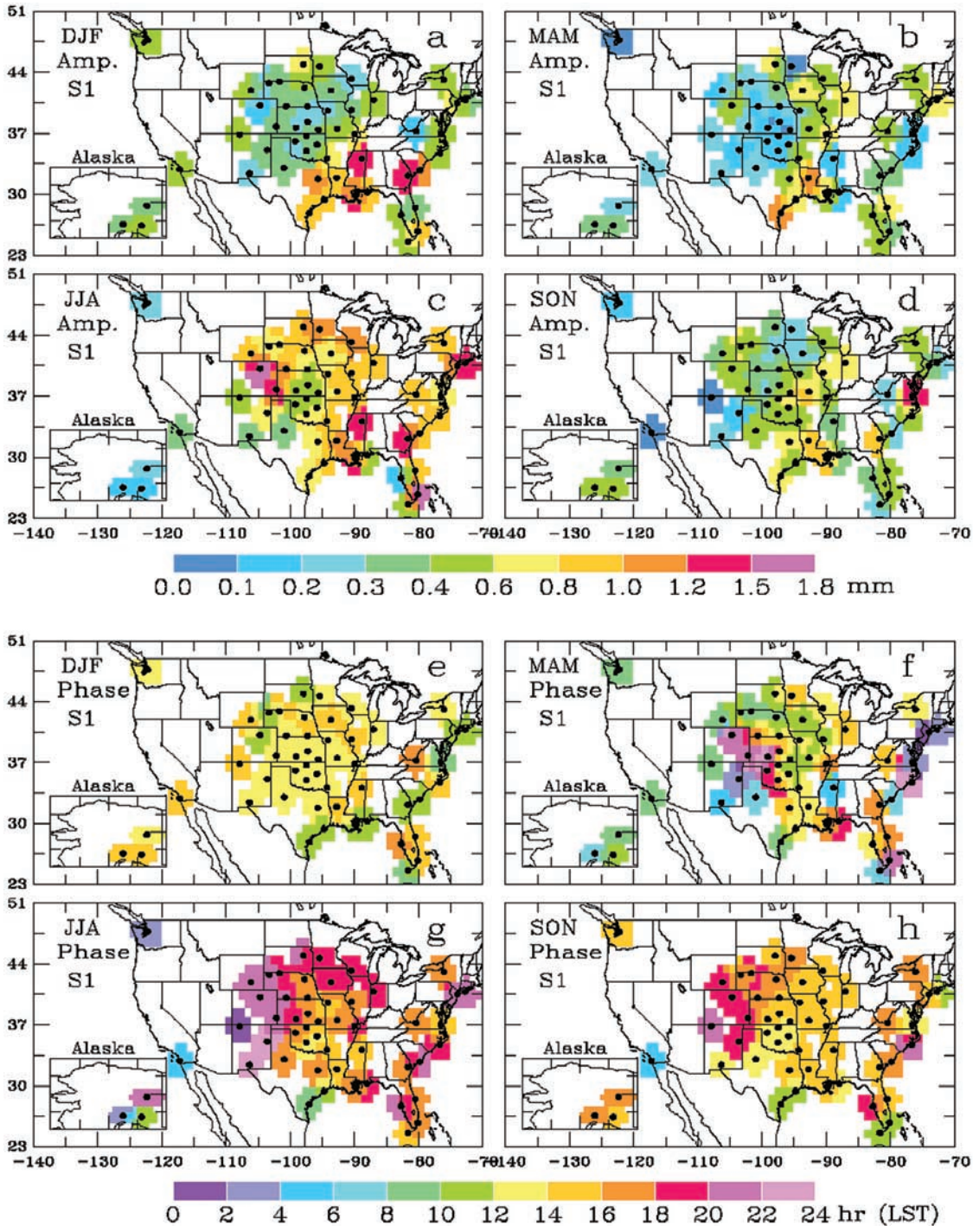

Figure 5. Spatial distribution of the (a–d) amplitude (mm) and (e–h) phase (LST at the maximum) of the diurnal harmonic of seasonal mean PW.

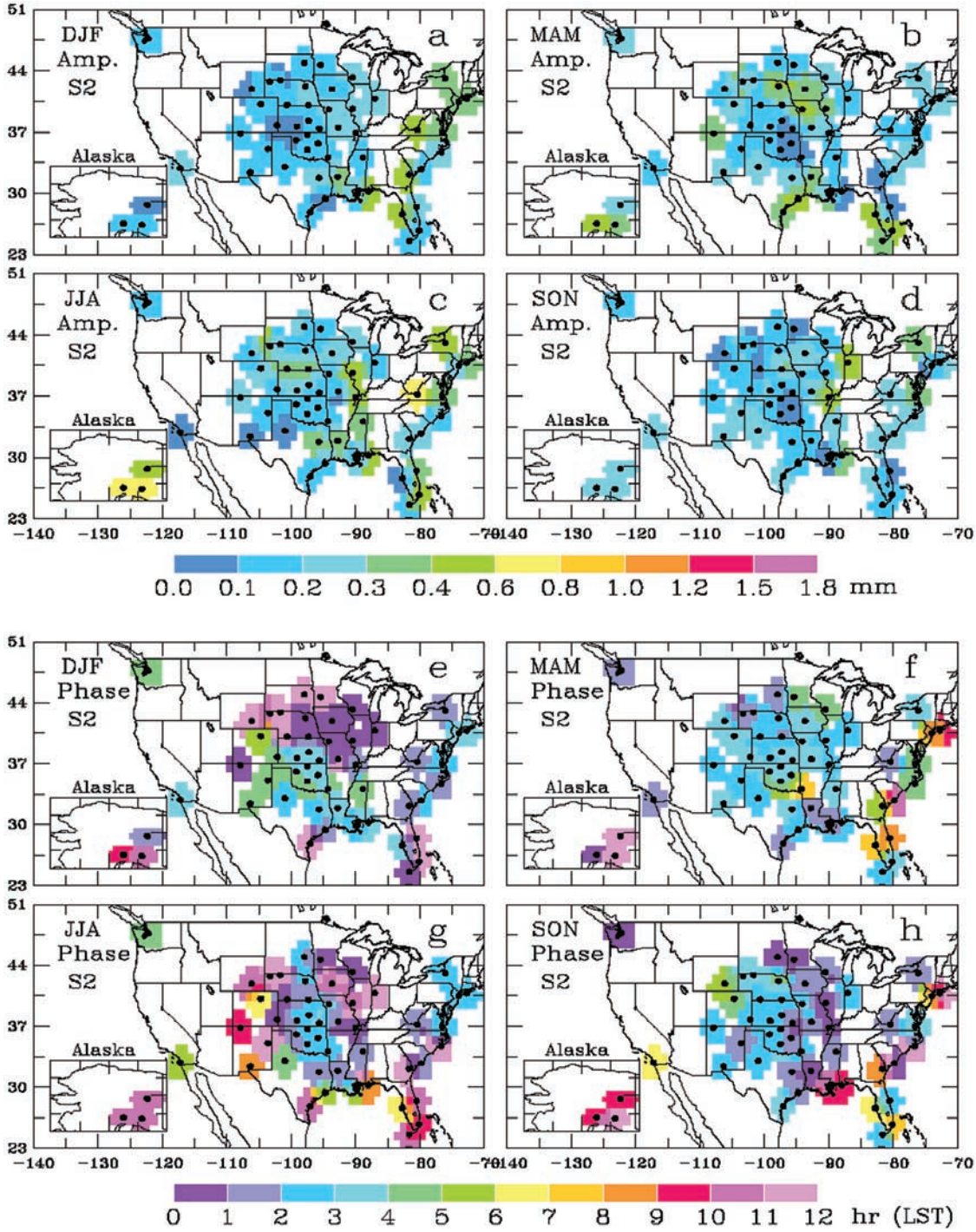

Figure 6. Same as in Figure 5 but for the semidiurnal harmonic. Phase is LST at the first maximum.

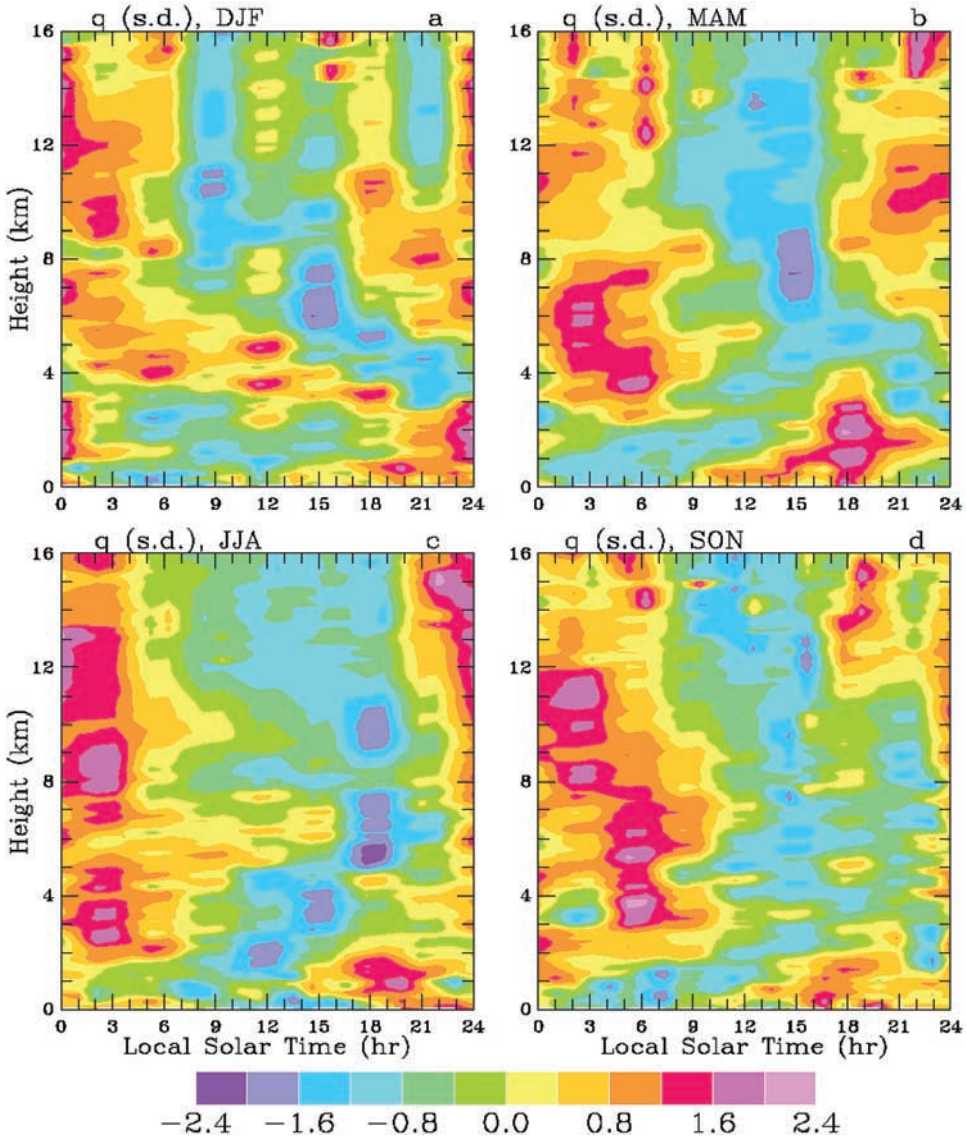

Figure 7. Seasonal mean diurnal anomalies (normalized by the standard deviation of the daily mean at each level) of atmospheric specific humidity derived from 3-hourly radiosonde data for 1994–2000 at the ARM/CART site near Lamont, Oklahoma. Number of days with eight soundings per day included in the averaging is 38 for DJF, 93 for MAM, 86 for JJA, and 92 for SON. Standard deviation of the daily mean for JJA ranges from ~0.50 g kg^{-1} at the surface to 0.76 g kg^{-1} around 1 km and <0.10 g kg^{-1} above 5.5 km.

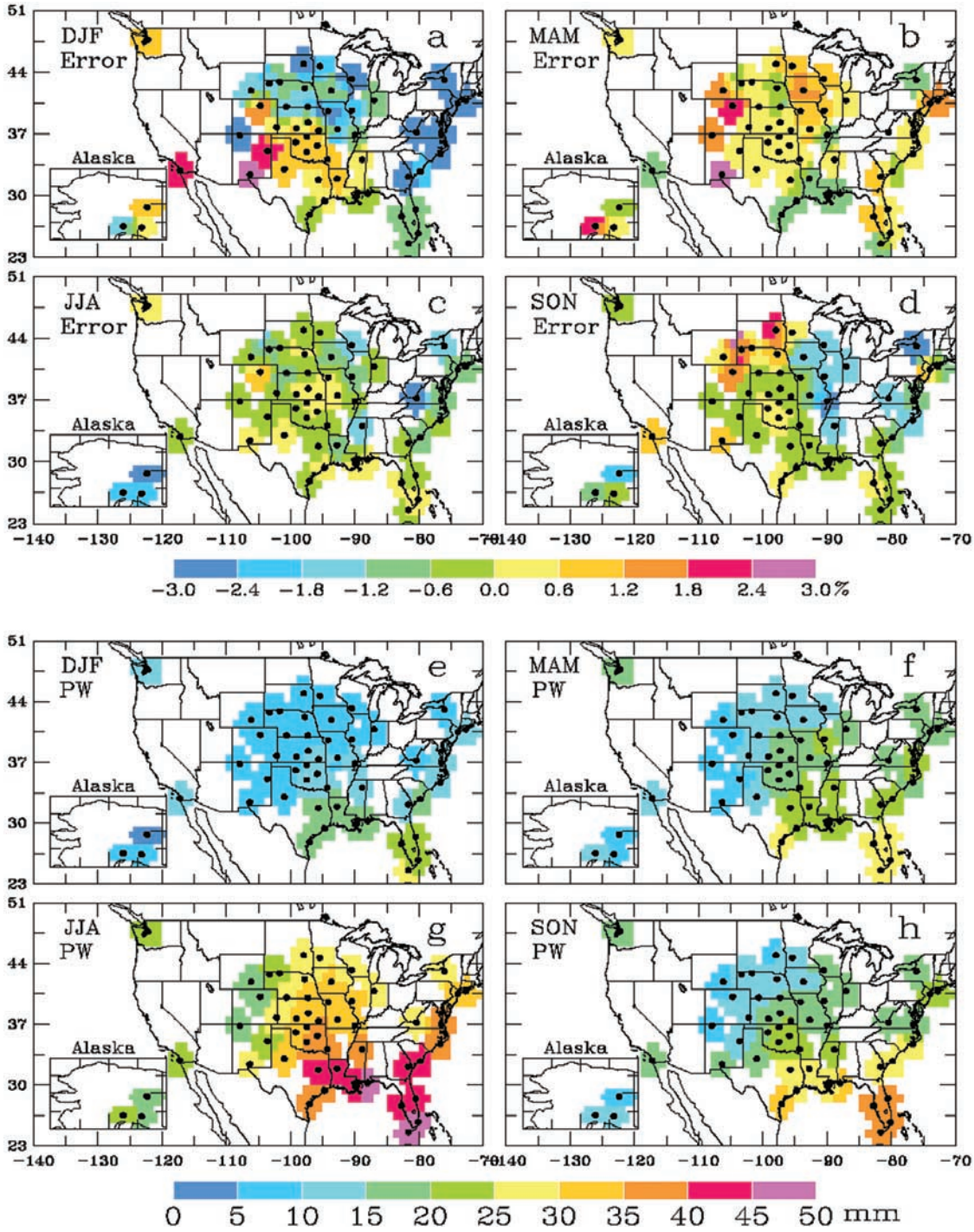

Figure 8. (a–d) Spatial distribution of the diurnal sampling error (percent) for twice (0000 and 1200 UTC) per day sampling and (e–h) seasonal mean PW derived from the 30-min GPS data (mm).